Bulletin of the Seismological Society of America, Vol. 97, No. 1B, pp. 151–161, February 2007, doi: 10.1785/0120050227

Crustal Attenuation within the Turkish Plateau and Surrounding Regions

by Ekrem Zor,* Eric Sandvol, Jiakang Xie, Niyazi Türkelli, Brian Mitchell, Arif H. Gasanov, and Gurban Yetirmishli

Abstract The lateral variations of seismic attenuation in the crust of Turkey and surrounding regions have been imaged from the inversion of interstation *Lg* *Q*-measurements.

This study develops the first tomographic model for *Lg* Q_0 in this region. That model is consistent with previous more qualitative *Lg*-attenuation models that showed inefficient or blocked *Lg* across the Eurasian-Arabian plate boundary. In general, the northern Arabian platform has low to normal *Lg* Q_0-values (~250–350), whereas high Q_0-values (~670–800) occur in the southern Arabian Plate. Additionally, we have found a dramatic decrease in *Lg* Q_0 across the Bitlis suture, the plate boundary between the Arabian and Eurasian plates. Beneath the Turkish Plateau, our high to moderate *Lg*-attenuation values (Q_0 ~100–200) probably originates from both scattering and intrinsic attenuation due to the tectonic complexity and the widespread young volcanics in the region. We conclude that the lowest Q_0-values for the East Anatolian plateau (~70–100) and the portion of western Turkey around the Menderes Massif (~60–150) are probably caused by intrinsic attenuation. We find low to normal *Lg* Q_0-values (~150–300) beneath the part of the Taurus Mountains in western Anatolia. These higher values may be related to the nature of the crust in the Tauride mountain belt. We also mapped the lateral variations in *Lg* η and observed a fairly consistent negative correlation between η and *Lg* Q_0 in the northern Middle East.

Introduction

Lg waves and their coda have been used successfully for the past three decades to infer and measure the attenuation structure of the crust (Nuttli, 1973; Kadinsky-Cade *et al.*, 1981; Xie and Nuttli, 1988; McNamara *et al.*, 1996; Mitchell *et al.*, 1997; Rodgers *et al.*, 1997; Cong and Mitchell, 1998; Mellors *et al.*, 1999; Philips *et al.*, 2000; Sandvol *et al.*, 2001). *Lg*, the most prominent phase over stable continental paths, is usually found in a group-velocity window between 3.6 and 3.0 km/sec at a frequency band of 0.2 to 5 Hz. It can be modeled as the sum of supercritical reflected *S* waves trapped within the crust (Herrin and Richmond, 1960; Bouchon, 1982) or as surface-wave overtones traveling in the continental crust (Knopoff *et al.*, 1973; Mitchell, 1995). *Lg* can be blocked when it propagates across (1) oceanic or very thin continental crust, (2) regions in which the wave-guide thickness changes rapidly, (3) deep sedimentary basins, or (4) regions of partial crustal melting (Ruzaikin *et al.*, 1977; Nuttli, 1980; Kennett, 1986; Bostock and Kennett, 1990; Baumgardt and Der, 1997; Rodgers *et al.*, 1997; Mitchell *et al.*, 1997; Xie *et al.*, 2004).

Different approaches have been used to quantify *Lg* propagation. Xie and Nuttli (1988) used a spectral ratio analysis of *Lg* coda to determine *Q*-values and found that their values were similar to those found by measuring direct *Lg* amplitudes. Later, Mitchell *et al.* (1997) and Cong and Mitchell (1998) successfully applied *Lg* coda *Q*-method to Eurasia and the Middle East. Because of the complexity of coda generation and propagation and other types of nonuniqueness in modeling coda such as the unclear role of modal conversions, several studies have used direct *Lg* waveforms processed with a two-station method (e.g., McNamara *et al.*, 1996; Xie *et al.*, 2004). Alternatively, Philips *et al.* (2000) and Sandvol *et al.* (2001) applied tomography to *Lg*/*Pg*-amplitude ratios. These methods assume that the source effects are canceled in the spectral ratio of the *Lg* and *Pg* phases. This approach has some difficulties in interpretation because of complexities in *Pg* propagation and the respective corrections (Philips *et al.*, 2000). Single-station methods have also been used by applying a correction for source size based on independent measures such as teleseismic m_b to account for the source contribution to *Lg* amplitudes. Using m_b directly to calculate seismic moment in regional studies may cause upper mantle bias in the *Q*-measurements (Marshall *et al.*, 1979; Philips *et al.*, 2000; Taylor *et al.*, 2003). Taylor *et al.* (2003) specified the source terms to absorb

*Present address: Earth and Marine Sciences Institute, TÜBİTAK, Marmara Research Center, 41470, Gebze, Kocaeli, Türkiye.

some of the problem with the m_b bias associated with source scaling. The strength of the two-station method is that one can eliminate the source effect to isolate path effect and calculate *Lg Q*, but the method may still have errors in removing the source effect in the case of nonisotropic source-radiation pattern with a nonzero alignment angle (Xie *et al.*, 2004). This study utilizes this method to eliminate most of the potential source contributions to our *Q*-measurements by using a small alignment angle.

This is the first study of frequency-dependent *Q* using direct *Lg* waves in the Middle East. It builds on observations of inefficient propagation and blockage in this region, but goes beyond those studies by quantifying the degree of attenuation along all paths. We have sufficiently dense data sets to actually measure the very low *Q*-values across the blockage zones such as the Bitlis suture.

Previous Attenuation Studies in the Region

In the past 25 years, many studies have been carried out in the Middle East to investigate crustal attenuation. Kadinsky-Cade *et al.* (1981) found *Lg* blockage across the Zagros fold and thrust belt. Rodgers *et al.* (1997) extended this region of *Lg* blockage into eastern Turkey. Mitchell *et al.* (1997) found that the lowest *Q*-values, <350, all lie within the Tethyan orogenic belt, which includes the Turkish-Iranian Plateau, and that moderately low *Q*-values are found in the Arabian Peninsula (350–500). Cong and Mitchell (1998) using $2^\circ \times 2^\circ$ cells found that Q_0 in Turkey is as low as 150. Mellors *et al.* (1999) found efficient *Lg* propagation across the Arabian shield. Gok *et al.* (2000) found that *Lg* does not propagate in northeast Anatolia, across the Lesser Caucasus and north of the South Aegean Trench. Using *Lg*/*Pg*-amplitude tomography, Sandvol *et al.* (2001) found evidence of a major increase in *Lg* attenuation across the Bitlis suture and Zagros fold and thrust belt and also outlined the boundary between the Arabian and Eurasian Plates. Al-Damegh *et al.* (2004) processed more data from the region and improved the *Lg*/*Pg* tomography map and found that *Lg* propagation within the Arabian plate is almost uniformly efficient whereas *Lg* propagation in the Turkish-Iranian Plateau is mostly blocked or inefficient. They also observed *Lg* blockage in the Mediterranean, which is consistent with the oceanic nature of most of the region. Sandvol *et al.* (2001) and Al-Damegh *et al.* (2004) also stated that the *Lg*/*Pg* ratios are higher along paths crossing the Arabian shield than along paths crossing the Eastern Arabian Plate.

Tectonic Setting

The Turkish plateau consists of a series of very complex tectonic terrains that span two separate plates: the Anatolian microplate and the Eurasian plate. The Turkish Plateau is surrounded by the African-Arabian plate to the south, the extension-dominated Aegean Sea domain to the west, and the Iranian Plateau to the east (Fig. 1).

In southwestern Turkey, the western Taurides contain three major nappe structures emplaced over the Tauride autochthonous rocks during the closure of the main Mesozoic Tethys (Neotethys) ocean in the Cretaceous. It has been suggested that the Taurus Mountains were uplifted in the Quaternary and may still be actively uplifting (Barka *et al.*, 1997). The Anatolian block is also composed of several crystalline massifs that are composed of exhumed orogenic middle crust such as the Menderes Massif (MM) in western Turkey (Whitney and Hamilton, 2004).

The Arabian Plate consists of a Precambrian shield bounded by sedimentary layers dipping eastward and reaching over 10 km in thickness (Powers *et al.* 1966; Mokhtar *et al.* 2001). Before the opening of the Red Sea, the Afro-Arabian and Eurasian plates were separated by the Neo-Tethys, which was being subducted beneath the Eurasian Plate. Continental collision along the Bitlis-Zagros suture zone (BZSZ) began in the early Miocene (Dewey *et al.*, 1973; Dewey and Sengor, 1979) and caused the westward movement of the Anatolian block between two prominent strike slip fault zones (Rotstein and Kafka, 1982), the left-lateral East Anatolian fault zone (EAFZ), and the right-lateral North Anatolian fault zone (NAFZ) (Fig. 1). The eastern Anatolian plateau (EAP) as a product of this collision is covered with late Cenozoic volcanics of diverse composition (Şengör and Kidd, 1979; Pearce *et al.*, 1990; Keskin, 2003). It is believed to be an elevated crustal block that is floating on partially molten, hot asthenospheric material. The ~2-km average elevation of EAP is not supported by simple Airy isostatic compensation; rather, the plateau is supported by low-density asthenospheric material (e.g., Şengör *et al.*, 2003). Also, the crust of eastern Turkey and a portion of the Lesser Caucasus appear hot and weak, and composed of crustal slivers that are in relative motion to one another (Barazangi *et al.*, 2005).

The Dead Sea Fault System (DSFS) constitutes the western boundary of the Arabian plate and extends from the Gulf of Aqaba (Eilat) in the south through to the Arabia-Eurasia collision zone in southern Turkey (Fig. 1). The DSFS formed as a result of the mid-Cenozoic rifting of Arabia from Africa (Garfunkel and Ben-Avraham, 1996) and is a boundary between the African and Arabian plates.

Data

We have collected waveform data from a wide variety of sources: permanent national networks, international seismological organizations in the area, and temporary stations deployed for research experiments. We used nine permanent broadband stations of Kandilli Observatory and Earthquake Research Institute National Network (KOERI) in Turkey, 2 permanent broadband stations of Lawrence Livermore National Observatory-Jordanian Seismic Observatory (LLNL-JSO), and 18 broadband stations of the Incorporated Research Institutions for Seismology (IRIS) Global Seismographic Network (GSN) which includes 12 GEOFON sta-

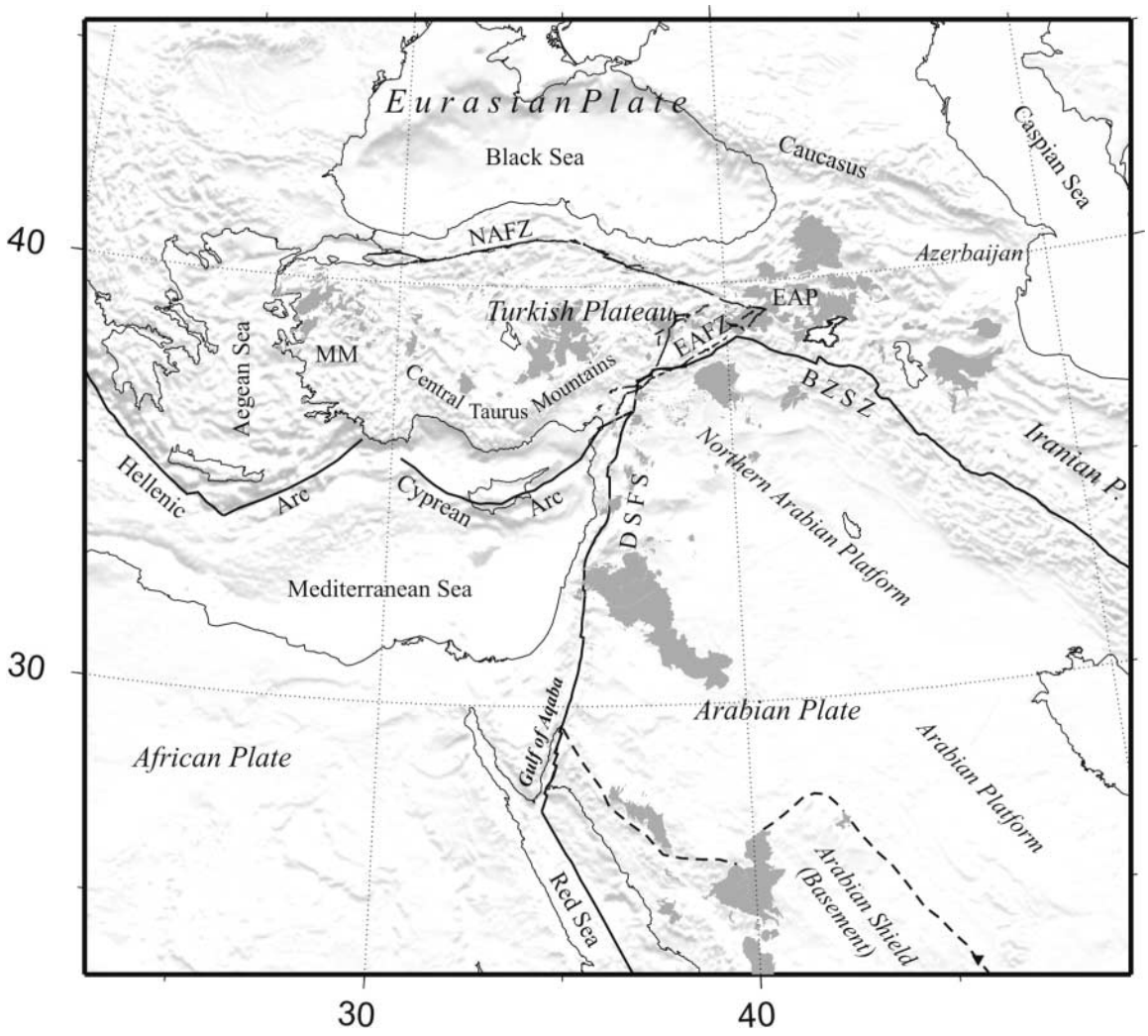

Figure 1. Map showing geographic locations of tectonic units in the study area. Solid and dashed lines show plate boundaries including major fault lines and the boundary of the Arabian shield, respectively. The North Anatolian fault zone (NAFZ), East Anatolian fault zone (EAFZ), Bitlis-Zagros suture zone (BZSZ), Dead Sea fault system (DSFS), the Menderes Massif (MM), and eastern Anatolian plateau (EAP) are also shown.

tions, 2 IRIS/IDA stations, 2 IRIS/USGS stations, 1 ETHZ station, and 1 MEDNET station. We also used 29 temporary broadband stations of the Eastern Turkey Seismic Experiment (ETSE), 4 temporary broadband stations of the Western Turkey Regional Network (WTRN), and 13 temporary broadband stations of the Azeri Seismic Network (ASN) (Fig. 2). When using a two-station approach, the contemporaneous coverage is important for obtaining the necessary number of two-station pairs. The data from these 75 broadband stations with reliable instrument responses were collected during the years 2002–2003 for KOERI, 1999–2001 for ETSE, 2002–2003 for WTRN, and 1999–2000 for LLNL stations. The overlapping periods of recording were used to form two station paths between KOERI-WTRN and ETSE-LLNL-JSO, as well as the GSN networks. We used approximately 2300 waveforms from ~200 events. All of our waveform data were sampled at a rate of least 20 samples per seconds. The ETSE, WTRN, and IRIS waveform data were recorded at 40 samples/sec, the LLNL-JSO data were recorded at 50 samples/sec while the KOERI and ASN data were recorded at 40 or more samples/sec.

Two-Station Method and Backprojection Tomography

We have employed methods to first estimate frequency-dependent *Lg Q* and then map its lateral variations using tomography. First, we applied a two-station method to estimate *Lg* Q_0 (Q at 1 Hz) and its power law frequency dependence (η) using the relationships given by Xie and Mitchell (1990b),

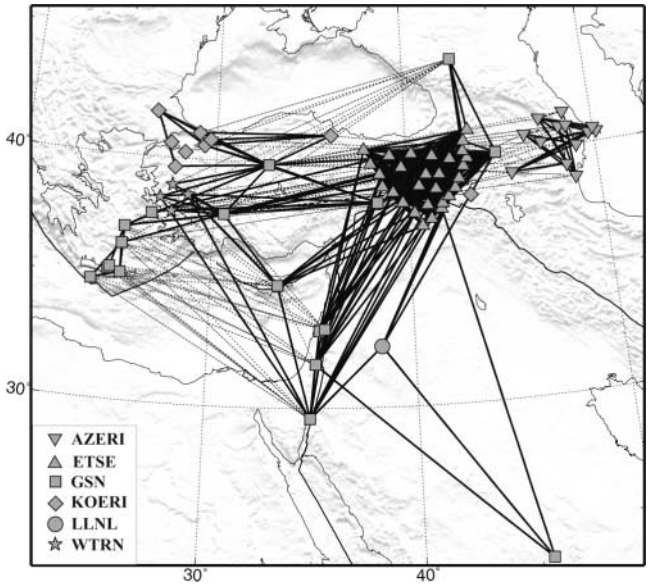

Figure 2. Two-station paths, for which we were able to estimate Q_0-values, used in the inversion process. The solid black and dashed lines show unblocked and blocked paths, respectively.

$$\ln\left[\frac{V_{Lg}}{\pi\Delta_{i,j}}\ln(R(f))\right] = (1 - \eta)\ln f - \ln Q_0 \qquad (1)$$

where $R(f)$ is,

$$R(f) = \left(\frac{\sqrt{\Delta_i}}{\sqrt{\Delta_j}}\right)\left(\frac{A_i(f)}{A_j(f)}\right), \qquad (2)$$

and V_{Lg} is the typical *Lg* group velocity 3.5 km/sec. Δ_i and Δ_j are the epicentral distance for each station, while $\Delta_{i,j}$ is the interstation distance between them. $A_i(f)$ and $A_j(f)$ are *Lg* spectra for each station. This method eliminates the source effect by taking the ratio of *Lg* spectra from the same source and also the geometrical spreading effect in one dimension by using the square root of the ratio of their epicentral distances. We estimated the interstation *Lg* Q_0 and η for the station pairs aligned with the source. These values may contain errors resulting from a nonisotropic source-radiation pattern, but this error should be minimal when using a small alignment angle. The successful isolation of the path effect also depends on the absence of complications in the propagation of the primary *Lg* wave such as forward scattering, focusing/defocusing, and nonunity site response caused by the three-dimensional structures in the real earth (Xie *et al.*, 2004). Therefore, *Q*-values, in almost all amplitude studies, may contain significant systematic uncertainties.

Second, these estimated *Lg* Q_0- and η-values associated with the interstation paths are used to map the lateral variations of these values by using a backprojection method (e.g., Xie and Mitchell, 1990a; Xie *et al.*, 2004). We divided the study region into discrete crustal cells and estimated the attenuation for each cell using the following linear relationship:

$$\frac{\Delta_n}{Q_n} = \sum_{m=1}^{M} \Delta_{mn} * Q_{mn}^{-1} + \varepsilon_n, \qquad (3)$$

where M is the total number of cells along the nth path, Q_{mn} is the *Lg* Q-value inside the mth cell to be inverted for, and ε_n is a small residual. Equation (3) is a set of N linear equations that can be solved using an iterative method.

Interstation *Lg Q* Measurements

We determined the possible two-station paths aligned with every source. We have used an angle $\delta\theta$, which is the difference between the azimuths from the source and the two stations to define the alignment. The choice of $\delta\theta_{\max}$ is less restrictive for *Lg* than for many other phases. Q_0 and η values may contain errors because of the effects of *Lg* attenuation outside the path and a nonisotropic source-radiation pattern using nonzero $\delta\theta$ (Xie *et al.*, 2004). To minimize this error, we chose to set $\delta\theta_{\max}$ to 15° as explained by Xie *et al.* (2004) based on results of Der *et al.* (1984). The second important parameter in this method is the interstation distance (Δ_{ij}). The potential error caused by Δ_{ij}, which is also strongly related to the estimated Q_0-value on the corresponding path, can be estimated by using the equation given by Xie *et al.* (2004):

$$\frac{\delta Q_0}{Q_0} \approx 1.1\left(\frac{Q_0}{\Delta_{ij}}\right)\delta x. \qquad (4)$$

To keep this error lower than 35% with a given modeling error value (δx) as 0.2, the interstation ratio between Q_0 and Δ_{ij} should not be greater than 1.6. By applying the criterion of $\delta\theta_{\max} = \pm 15°$ and the interstation ratio = 1.6 to the ~2300 *Lg* spectra, we have found 1383 two station paths from ~140 regional events (Fig. 2). When calculating *Lg* Q_0 and η, we did not fix the *Lg* window on the waveform because *Lg* velocity typically varies by 20% from one region to another as emphasized by Nuttli (1973). From nine examples of two-station paths in Figure 3, we show six waveform examples of how we determined Q_0 (*Lg* Q at 1 Hz) and picked the *Lg* window in Figures 4 and 5. Having picked the *Lg* windows, we have taken the ratio of two station *Lg* spectra and the epicentral distances using equation (2) to eliminate the source and the one-dimensional geometrical spreading effect. Finally, we obtained *Lg* Q_0 and η using a linear regression fitting based on equation (1).

In Figure 4, we show three waveform examples from the interstation paths crossing the Arabian Plate where we have found the highest *Lg* Q_0-values (~600–800). These interstation paths can be seen in Figure 3 and are labeled as

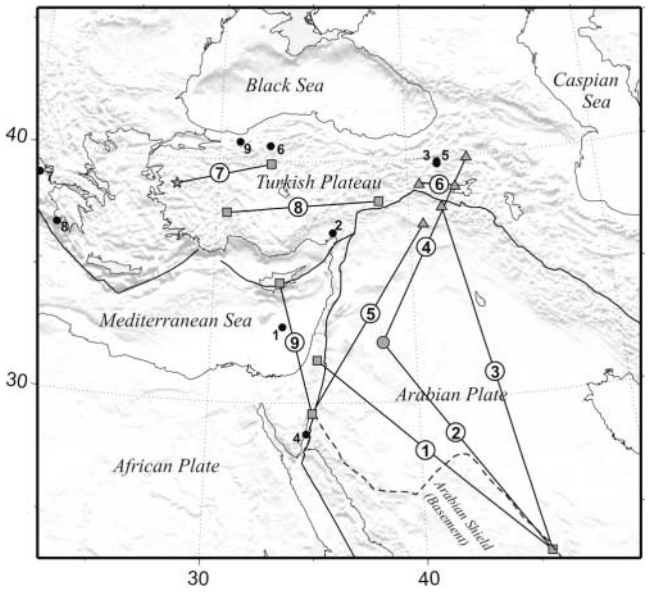

Figure 3. Some examples of two-station paths. Black dots show events that were used to measure Q from the related two-station paths on the map. The events and the related paths were labeled with the same numbers. Station symbols are the same as in Figure 2. Solid and dashed lines show the boundaries of the plates and Arabian shield, respectively.

2 for stations RUW-RAYN (Fig. 4a), 3 for KTLN-RAYN (Fig. 4b), and 4 for RUW-CMCY (Fig 4c). High *Lg* Q_0-values were measured in the southwestern part of Arabian Plate for the stations RUW-RAYN (~800). Also, we observe similar value for another station pair JER-RAYN (~800), which is labeled as 1 in Figure 3. These high values are most probably due to the lack of a substantial low-velocity sedimentary layer in the Arabian shield. We also measure a lower Q_0-value for the stations KTLN-RAYN (~550). This path is crossing the northern and southern Arabian platform where the sedimentary layer is thicker (~5–15 km). We also observe low to normal *Lg* Q_0-values (~350) for the paths crossing the northern Arabian platform such as path 5 (Fig. 3). Note also the much lower *Lg* Q_0-value ~190 for the interstation path RUW-CMCY, which crosses the Bitlis suture. This indicates a very dramatic increase in the level of attenuation across the Arabian-Eurasian plate boundary. Exceptionally low Q_0-values were measured for a fairly large region of the eastern Anatolian plateau in this plate boundary (~70–100).

The Turkish Plateau also shows some significant variations in *Lg* Q_0-values (~60–315). In Figure 5, the two sample waveforms are shown from this region where we observe lowest *Lg* Q_0-values. Their interstation paths are labeled as 6 for the stations BNGL-AHLT (Fig. 5a) and 7 for the stations AKH-ANTO (Fig. 5b). The very low Q_0-values in the eastern Anatolian plateau such as the stations BNGL-AHLT (~70) and the portion of western Turkey around the Menderes Massif such as the stations AKH-ANTO (~90) are most probably due to the widespread Quaternary volcanism. There is also ongoing extension in western Turkey, especially beneath the Menderes Massif.

We also show two interesting interstation paths crossing the western Taurus Mountains in southern Anatolia and the eastern Mediterranean. Exceptionally low to normal *Lg* Q_0-values have also been found for the station ISP-MALT (~150–315) and CSS-EIL (~300) which are labeled as 8 and 9 in Figure 3, respectively. The relatively higher values beneath western Taurus Mountains may be related to the root of the mountain. In the eastern Mediterranean, we observe what appears to be a relatively fast (3.9 km/sec group velocity) phase at station EIL for the interstation path between CSS-EIL (Fig. 5c). It is not classified as *Sn*, because it arrives much later than a typical *Sn*. The usual *Sn* window is plotted in the figure using the upper mantle velocity between 4.5 and 4.7 km/sec. As is evidenced by its relatively fast group velocity and its path through oceanic crust, this energy is most probably from *Sn* to *Lg* converted energy. The conversion most probably occurs along the northern coast of the Sinai, west of the southern Dead Sea Fault System. This conversion will bias our Q-measurements upward along the eastern Mediterranean. Note, however, that the *Lg* Q-values are consistent with the number we have obtained from the DSFS region.

Mapping Variations in *Lg* Q_0 and η

Of the 1383 two-station pairs, those paths with higher standard deviations (>50%) from the linear regression were excluded from the tomography. We have a total of 694 observations from 296 unblocked two-station paths with stable *Lg* Q_0-values and 263 observations from 154 two-station paths with blocked *Lg*. We have defined a two-station blocked *Lg* path as a two-station pair where *Lg* is observed at the closest station and then not observed at the more distant station. Hence, we know that the *Lg* blockage is occurring between the two stations. After averaging repeated observations from 296 unblocked two-station paths, the resulting *Lg* Q_0-values were used to obtain a laterally varying Q_0-model as shown in Figure 6a using a $1^\circ \times 1^\circ$ cell size. We used the average *Lg* Q_0 of 148 for the initial constant Q_0-model for the study area. One hundred ninety-eight cells were sampled and used from the total of 720. The variance reduction is 43% over an initial constant Q-model, corresponding to 70% variance reduction in predicted amplitudes. Although stable measurements of interstation η-values are much more difficult to obtain than those of Q_0-values as stated by Xie *et al.* (2004), an attempt has been made to invert for laterally varying η-values and its deviation from the linear regression in the Middle East (see Fig. 7a,b).

To increase path coverage and resolution, we supplemented the 296 unblocked paths with 154 blocked paths for the second tomographic model (Fig. 6c). To estimate the

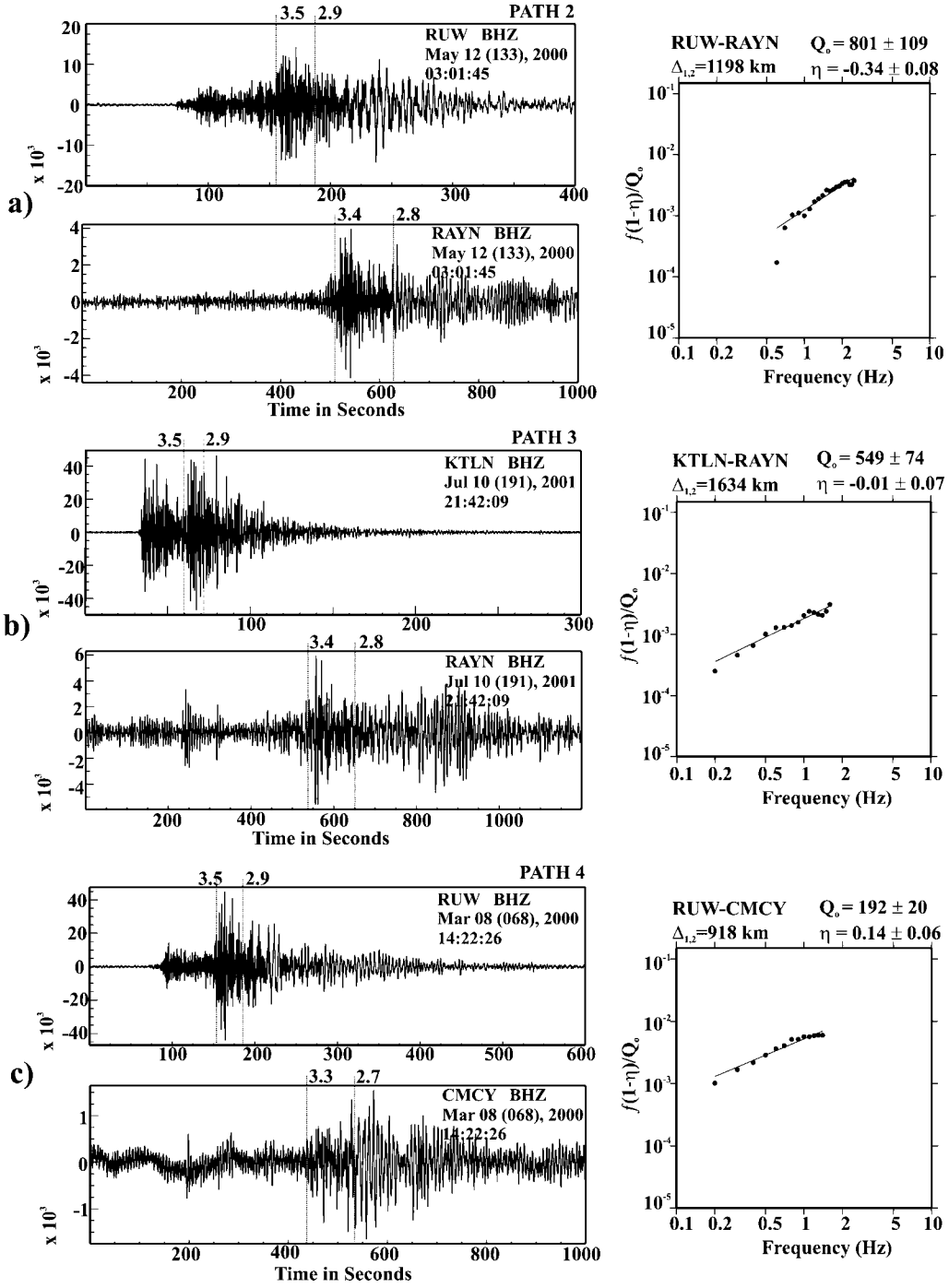

Figure 4. Examples of waveforms (left-hand panels) and linear regression determination of *Lg Q* (right-hand panels) for paths crossing the Arabian Plate. Numbered dashed lines show the *Lg* group velocity window. (a) RUW-RAYN, (b) KTLN-RAYN, and (c) RUW-CMCY. Path numbers as in Figure 3 are also shown on the waveform panels.

Q-values for these blocked paths, we used the equation below:

$$\frac{V_{Lg}}{\pi\Delta_{ij}} \ln\left(\left(\frac{\sqrt{\Delta_i}}{\sqrt{\Delta_j}}\right)A_{\text{loss}}\right) = f^{1-\eta}/Q_0.$$

We assumed $V_{Lg} = 3.5$ km/sec and $A_{\text{loss}} = 99.0$. This represents a 99% amplitude loss from the first (*i*th) station to the second (*j*th) for $f = 1$ Hz. We term this value the maximum allowable *Lg* Q_0. Of course the actual Q_0-value is most probably less than this value. The total of 450 two-station paths were inverted in the second inversion. The tomographic model is shown in Figure 6c with an average *Lg* Q_0

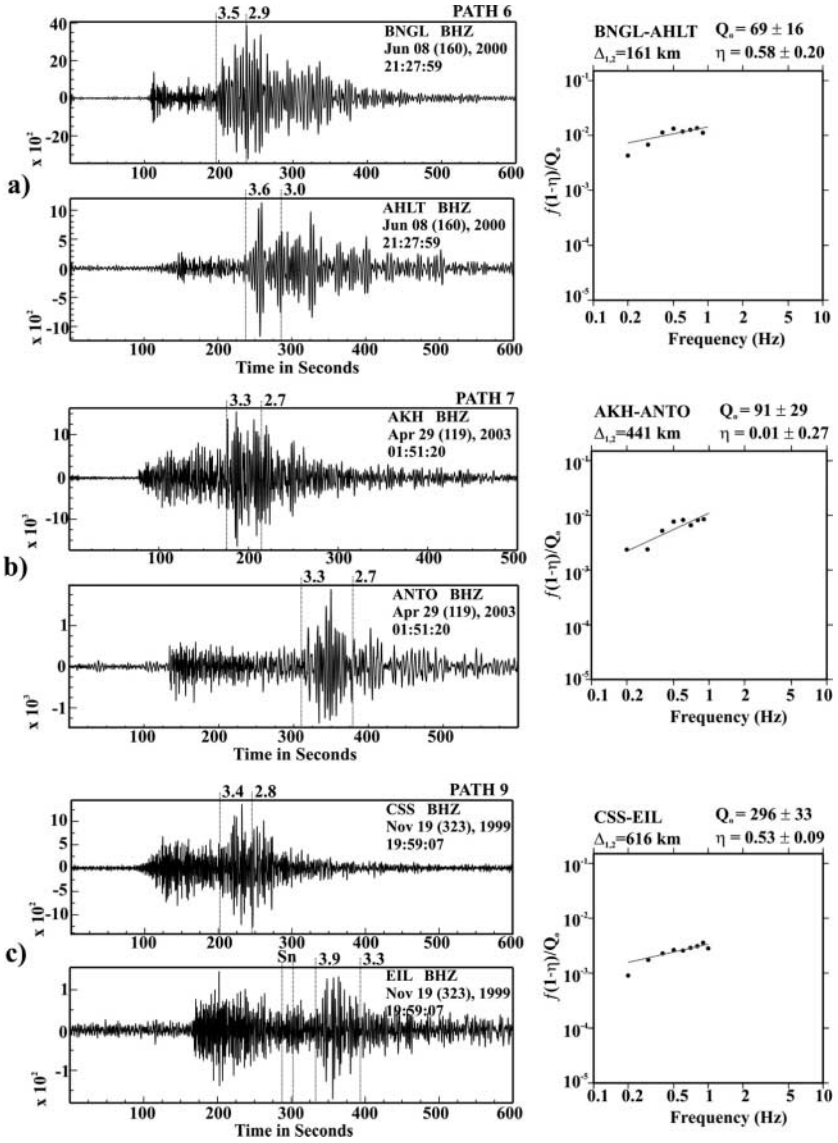

Figure 5. Examples of waveform and linear regression determination of *Lg Q* for the paths in the Turkish Plateau and Mediterrenean regions. Numbered dashed lines show the *Lg* group velocity window. (a) BNGL-AHLT, (b) AKH-ANTO, and (c) CSS-EIL. Path numbers as in Figure 3 are also shown on the waveform panels. The *Sn* window is also calculated using the velocity between 4.5 and 4.7 km/sec and plotted on (c).

of 177 as an initial constant model. The variance reduction is 44%, corresponding to 64% variance reduction in predicted amplitudes over an initial constant *Q*-model.

The resolution was examined using a two-dimensional checkerboard pattern of low and high *Q*-anomalies. Attenuation perturbations of $\pm 20\%$ with $\pm 5\%$ normally distributed random noise were used to calculate a synthetic data set. By using a series of checkerboards with different cell sizes, we estimated that the smallest easily distinguished cell size is $2^\circ \times 2^\circ$. The checkerboard test results for the first and second tomographic inversion are shown in Figures 6b and d, respectively. As can be seen from the figures, we have excellent resolution for the areas where we have excellent coverage in terms of crossing rays. In the areas where we do not have enough crossing rays, we observe significant smearing.

Discussion and Conclusions

In this study, we processed a large set of new broadband waveform data to obtain an *Lg Q* model for much of the Middle East. The resulting tomographic model in Figure 6a clearly shows the variations in *Lg Q* across plate boundary between the Arabian Plate and the Turkish Plateau portion of the Eurasian Plate. In general, the *Lg* Q_0-values are higher within the Arabian Plate than beneath the Turkish Plateau. Other studies have also concluded that *Lg* propagation in the Turkish-Iranian Plateau is usually blocked or highly attenuated (Sandvol *et al.*, 2001; Al-Damegh *et al.*, 2004). We also observe substantial variation in *Lg* Q_0-values within the Arabian Plate itself; we observe higher values beneath the Arabian shield than beneath the Arabian and northern Arabian Platform. These higher values could potentially be due,

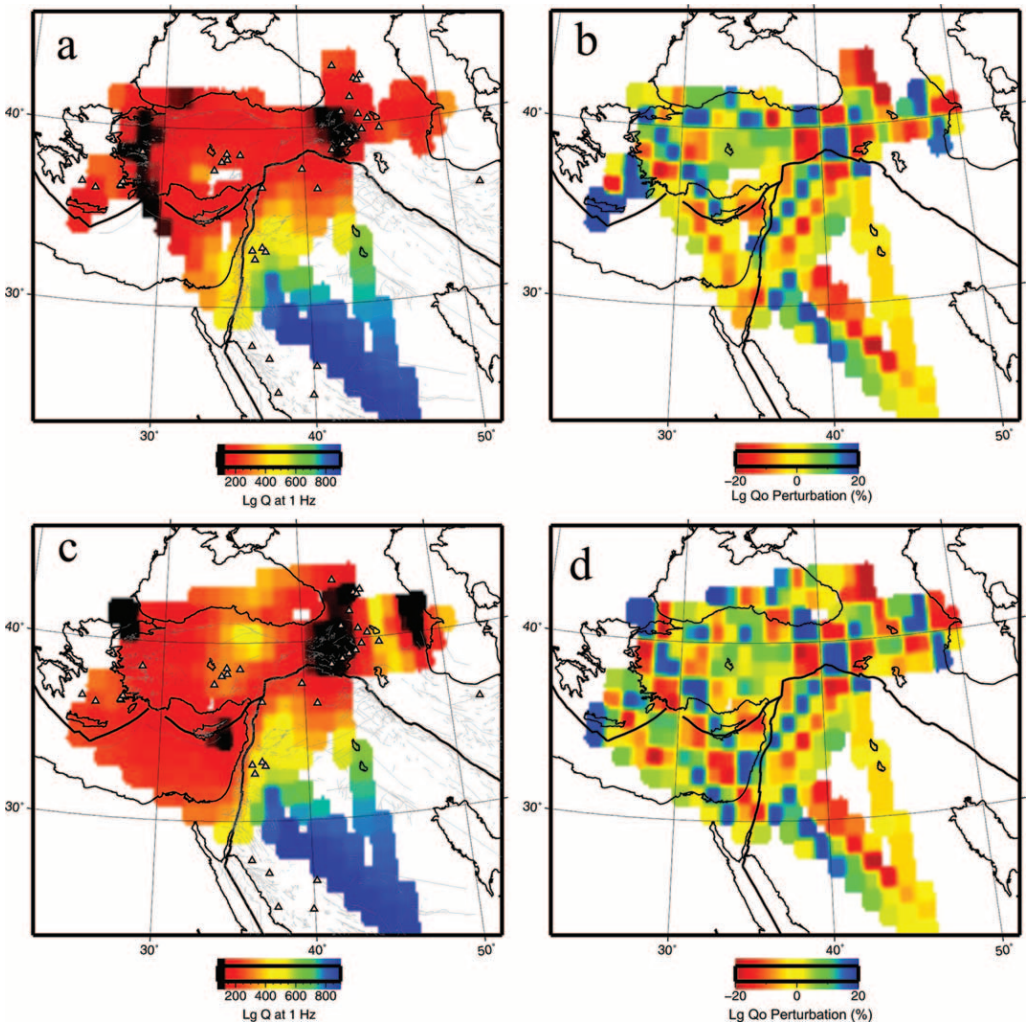

Figure 6. Tomographic inversion result for 296 unblocked two-station paths (a) and 450 two-station paths which includes 296 unblocked and 154 blocked paths (c). Their resolutions for 2° × 2° checkerboard model are shown on the right as panels (b) and (d), respectively. The estimated *Lg* Q_0 values were inverted with the 1° × 1° cell size. Triangles and solid lines indicate seismic stations used in this analysis and plate boundaries, respectively.

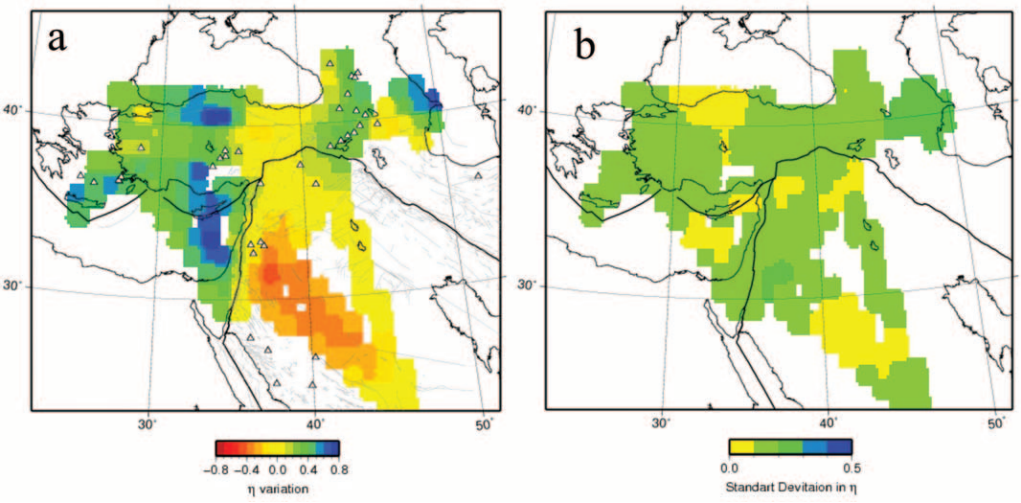

Figure 7. Lateral variation of the power law frequency dependence (η) of *Lg* Q_0 (a) and its deviation by linear regression fitting (b).

in part, to systematic errors given the lack of crossing paths in this portion of our model. Similarly, the Turkish Plateau also shows some significant variations in crustal attenuation, with normal *Lg* Q_0-values observed beneath the Central Taurus Mountains and very low *Lg* Q_0-values beneath the eastern Anatolian plateau and western Turkey around the Menderes Massif. Of course some subregions are not sampled by the two-station paths because of the lack of stations in central Anatolia from south to north.

High *Lg*-attenuation values within the Anatolian plateau (Q_0 ~100–200) may be caused by a combination of scattering and intrinsic attenuation. Scattering attenuation is due to the tectonic complexity and the intrinsic attenuation could be due to the widespread crustal melting. However, the lowest Q_0-values in eastern Anatolian plateau (~70–100) and the portion of western Turkey around the Menderes Massif (~60–150) are most probably due to the widespread Quaternary volcanism. In western Turkey, there is a correlation with the location of the young volcanism and the geothermal activity (İlkişik, 1995; Göktürkler *et al.*, 2003). Zhu *et al.* (2006) have shown that the crustal thickness of western Turkey probably does not change rapidly enough to reduce or block the *Lg* phases. Similarly, the receiver function waveform inversion in eastern Turkey has suggested that there is no rapid change in the crustal thickness across the Bitlis Suture and East Anatolian Fault Zone. They also observed localized midcrustal seismic, low-velocity zones scattered throughout the eastern Anatolian plateau. These low-velocity zones might be an indication of partial melt within the eastern Turkey crust (Zor *et al.*, 2003). This inference is also supported by the widespread, young (less than 6 Ma) volcanism in the region (e.g., Keskin, 2003) and low *Pn* velocities (Hearn and Ni, 1994; Al-Lazki *et al.*, 2004) coupled with high *Sn* attenuation (Gok *et al.*, 2003; Al-Damegh *et al.*, 2004) as an indication of anomalously hot lithosphere. Another region where low *Lg* Q_0-values have been found to coincide with low crustal velocity is central and southern Tibet. Xie *et al.* (2004) observed low *Lg* Q_0-values of ~100 in central Tibet and extremely low *Lg* Q_0-values of ~60–70 in southern Tibet. Similar midcrustal, low-velocity zones have also been found in the southern Tibetan crust.

Beneath the western Taurus Mountains in southern Anatolia, exceptionally low to normal *Lg* Q_0 values (~150–300) have also been found. These relatively higher values may be related to the root of the mountain that would comprise a stable continental crustal waveguide as in southernmost Tibet in the general region of high Himalayas (>300) (Xie *et al.*, 2004). Furthermore, the sedimentary cover is limited in this region, which might also improve the efficiency of *Lg* propagation in this region. It is important to note that our paths are all parallel to the strike of the mountain front. Gok *et al.* (2000) suggest that paths that are perpendicular to the Taurides tend to be inefficient or blocked. We were unable to test this because of the lack of perpendicular two-station paths in this region. For northeastern Turkey, the Caucasus, and Azerbaijan, we also found some low to normal *Lg* Q_0-values (~170–180) as well as some blocked two-station paths.

We found large variations in *Lg* Q_0 for paths crossing the Arabian Peninsula (~300–800). Our *Lg* Q_0-values are roughly consistent with the observations from *Lg* coda Q (350–500) by Mitchell *et al.* (1997) and Cong and Mitchell (1998). However, they did not observe such high *Lg* Q_0-values like ~800 in the Arabian Plate. This slight inconsistency may be caused by the difference in sampling area between direct *Lg* and *Lg* coda. However, note that we have very few paths crossing the Arabian shield for which we have found higher *Lg* Q_0-values. Therefore, systematic errors caused by the effect of lateral changes in the crustal structure may have a large effect on our measurements. The northern Arabian platform crust has low to normal *Lg* Q_0-values (~300–350). In addition, we observe high Q_0 (~670–800)-values for the southern Arabian Plate where previous *Lg*/*Pg* studies show little attenuation. This is most probably due to the lack of any substantial sedimentary cover in the Arabian shield. We also observe lower Q-values (~550) for paths crossing the northern and southern Arabian platform where the sedimentary layer is thicker than the western Arabian plate. Additionally, we have found a dramatic decrease in *Lg* Q_0 across the Arabian-Eurasian plate boundary. This is due to a fundamental difference in the rheology of Anatolian crust compared with the Arabian crust. Paths to the south of the Bitlis suture have *Lg* Q_0-values of ~350–550, but the paths crossing the Bitlis suture have an *Lg* Q_0 of ~200. This decrease may be related to the higher intrinsic attenuation due to partial melt in eastern Anatolian Plateau. Furthermore, the Anatolian crust is composed of a very complex series of accreted terrains with a large number of active fault zones. Earlier studies similarly observe *Lg*-amplitude reductions over paths crossing the boundaries of the large plateaus like Tibet (Ruzaikin *et al.*, 1977; Ni and Barazangi, 1983).

We have observed apparently inefficient *Lg* propagation across the southeastern Mediterranean with high group velocity (~3.9 km/sec). This apparently fast *Lg* propagation is probably due to *Sn* to *Lg* conversion as discussed by Seber *et al.* (1996). We see high Q_0-values for this area in the first tomographic model (Fig. 6a), but the Mediterranean region is represented by low Q_0 in the second tomography model (Fig. 6c) because of the blocked paths via the maximum allowable Q_0-values (the true Q_0-values are most likely to be lower). The primary difference in the two models is due to the higher density of blocked paths in the Mediterranean Sea.

We also have attempted to map the lateral variation in η (Fig. 7a) for the northern Middle East. The average η is anomalously low for the entire Middle East (0.25). We also found a fairly consistent pattern with our *Lg* Q_0 map (Fig. 6a). Low η-values correlate with high values of Q_0 in the Arabian Plate. The inverse relationships between Q_0 and η have been previously observed for northern India and in a region north of Caspian Sea by Mitchell *et al.* (1997). They

also have been reported by Nuttli (1988) and Mitchell (1995). Figure 7b also shows our map of η deviation by the linear regression fitting. The large regions of negative η covering much of the Arabian plate may be caused by the limited frequency range used to calculate η in regions of high Q.

Acknowledgments

This work was supported by a grant for the U.S. Department of Energy DE-FC52-903NA99518. This work benefited greatly from discussion with Arthur Rodgers and Muawia Barazangi. Furthermore, Arthur Rodgers helped us obtain data from two stations in Jordan. We thank IRIS, from which we accessed a large portion of our waveforms. We also thank GEOFON, MEDNET, the ETHZ Swiss seismological service, Project IDA at the University of California San Diego, the U.S. Geological Survey Albuquerque Seismological Laboratory, and GSN (operated by IRIS, USGS, and NSF) as data providers to IRIS. We also thank Christine Sandvol for editing.

References

Al-Damegh, K., E. Sandvol, A. Al-Lazki, and M. Barazangi (2004). Regional seismic wave propagation (Lg and Sn) and Pn attenuation in the Arabian Plate and surrounding regions, *Geophys. J. Int.* **157,** 775–795.

Al-Lazki, A., E. Sandvol, D. Seber, M. Barazangi, N. Turkelli, and R. Mohamad (2004). Pn tomographic imaging of mantle lid velocity and anisotrophy at the junction of the Arabian, Eurasian and African plates, *Geophys. J. Int.* **158,** 1024–1040.

Barazangi, M., E. Sandvol, and D. Seber (2006). Structure and tectonic evolution of the Anatolian Plateau in eastern Turkey, in *Postcollisional Tectonics and Magmatism in the Mediterranean Region and Asia: Geological Society of America Special Paper 409*, Y. Dilek and S. Pavlides (Editors).

Barka, A., and R. Reilinger (1997). Active tectonics of the eastern Mediterranean region: deduced from GPS, neotectonic and seismicity data, *Ann. Geofis.* **40,** 587–610.

Baumgardt, D. R., and Z. Der (1997). Investigation of the Transportability of the P/S ratio discriminant to different tectonic regions, *Science Report* **1,** PLT-TR-94-229, ENSCO, Inc., Springfield, Virginia.

Bostock, M. G., and B. L. N. Kennett (1990). The effect of 3D structure on Lg propagation patterns, *Geophys. J. Int.* **101,** 355–365.

Bouchon, M. (1982). Complete synthesis of seismic crustal phases at regional distances, *J. Geophys. Res.* **87,** 1735–1741.

Cong, L., and B. Mitchell (1998). Lg coda Q and its relation to the geology and tectonics of the Middle East, *Pure Appl. Geophys.* **153,** 563–585.

Der, Z., M. E. Marshal, A. O'Donnell, and T. W. McElfresh (1984). Spatial coherence structure attenuation the Lg phase, site effects, and interpretation of the Lg coda, *Bull. Seism. Soc. Am.* **74,** 1125–1148.

Dewey, J. F., and A. M. C. Sengor (1979). Aegean and surrounding regions: complex multiplate and continuum tectonics in a convergence zone, *Geol. Soc. Am. Bull.* **90,** 84–92.

Dewey, J. F., W. Pitman, W. Ryan, and J. Bonnin (1973). Plate tectonics and the evolution of the Alpine system, *Geol. Soc. Am. Bull.* **84,** 3137–3180.

Garfunkel, Z., and Z. BenAvraham (1996). The structure of the Dead Sea basin, *Tectonophysics* **266,** 155–176.

Gok, R., N. Türkelli, E. Sandvol, D. Seber, and M. Barazangi (2000). Regional wave propagation in Turkey and surrounding regions, *Geophys. Res. Lett.* **27,** 429–432.

Gok, R., E. Sandvol, N. Turkelli, D. Seber, and M. Barazangi (2003). Sn attenuation in the anatolian and Iranian plateaus and surrounding regions, *Geophys. Res. Lett.* **30,** 8042, doi 10.1029/2003GL018020.

Göktürkler, G., M. Salk, and C. Sari (2003). The numerical modelling of the conductive heat flow in western Anatolia, *J. Balkan Geophys. Soc.* **6,** 1–15.

Hearn, T., and J. Ni (1994). Pn velocities beneath continental collision zones: the Turkish-Iranian Plateau, *Geophys. J. Int.* **117,** 273–283.

Herrin, E. T., and J. Richmond (1960). On the propagation of the Lg phase, *Bull. Seism. Soc. Am.* **50,** 197–210.

İlkişik, O. M. (1995). Regional heat flow in western Anatolia using silica temperature estimates from thermal springs, *Tectonophysics* **244,** no. 1–3, 175–184.

Kadinsky-Cade, K., M. Barazangi, J. Oliver, and B. Isacks (1981). Lateral variation in high frequency seismic wave propagation at regional distances across the Turkish-Iranian plateaus, *J. Geophys. Res.* **86,** 9377–9396.

Kennett, B. L. N. (1986). Lg waves and structural boundaries, *Bull. Seism. Soc. Am.* **76,** 1133–1141.

Keskin, M. (2003). Magma generation by slab steepening and breakoff beneath a subduction-accretion complex: an alternative model for collision-related volcanism in Eastern Anatolia, Turkey, *Geophys. Res. Lett.* **30,** no. 24, 8046, doi 10.1029/2003GL018019.

Knopoff, L., F. Schwab, and E. Kausel (1973). Interpretation of Lg, *Geophys. J. R. Astr. Soc.* **33,** 289–404.

Marshall, P. D., D. L. Springer, and H. C. Rodean (1979). Magnitude corrections for attenuation in the upper mantle, *Geophys. J. R. Astr. Soc.* **57,** 609–638.

McNamara, D. E., T. J. Owens, and W. R. Walter (1996). Propagation characteristics of Lg across the Tibetan Plateau, *Bull. Seism. Soc. Am.* **86,** 457–469.

Mellors, R., F. Vernon, V. Camp, A. Al-Amri, A. Ghalib, and M. Al-Dail (1999). Regional wave propagation in the Saudi Arabian peninsula, *Geophys. Res. Lett.* **104,** 20,221–20,235.

Mitchell, B. J. (1995). Anelastic structure and evolution of continental crust and upper mantle from seismic surface wave inversion, *Rev. Geophys.* **33,** 441–462.

Mitchell, B. J., Y. Pan, J. Xie, and L. Cong (1997). Lg coda Q variation across Eurasia and its relation to crustal evolution, *J. Geophys. Res.* **102,** 22,767–22,779.

Mokhtar, T. A., C. J. Ammon, R. B. Herrman, and H. A. A. Ghalib (2001). Lithospheric structure beneath Arabia, *Pure Appl. Geophys.* **158,** 1445–1474.

Ni, J., and M. Barazangi (1983). High frequency seismic wave propagation beneath the Indian Shield, Himalayan Arc, Tibetan Plateau and surrounding regions: high uppermost mantle velocities and efficient Sn propagation benath Tibet, *Geophys. J. R. Astr. Soc.* **72,** 665–689.

Nuttli, O. W. (1973). Seismic wave attenuation and magnitude relations for eastern North America, *J. Geophys. Res.* **78,** 5212–5218.

Nuttli, O. W. (1980). The excitation and attenuation of seismic crustal phases in Iran, *Bull. Seism. Soc. Am.* **70,** 469–485.

Nuttli, O. W. (1988). Lg magnitudes and yield estimates for underground Novaya Zemlya nuclear explosions, *Bull. Seism. Soc. Am.* **78,** 873–884.

Pearce, J. A., J. F. Bender, S. E. De Long, W. S. F. Kidd, P. J. Low, Y. Guner, F. Saroglu, Y. Yilmaz, S. Moorbath, and J. G. Mitchell (1990). Genesis of collision volcanism in Eastern Anatolia, Turkey, *J. Volcanol. Geotherm. Res.* **44,** 189–229.

Philips, W. S., H. E. Hartse, and S. R. Taylor (2000). 1 Hz Lg Q tomography in central Asia, *Geophys. Res. Lett.* **20,** 3425–3428.

Powers, R. W., L. F. Ramirez, C. P. Redmond, and E. L Elberg (1966). Geology of the Arabian peninsula: sedimentary geology of Saudi Arabia, *U.S. Geol. Surv. Profess. Pap. 560-D*, 91–96.

Rodgers, A., J. Ni, and T. Hearn (1997). Propagation characteristics of short period Sn and Lg in the Middle east, *Bull. Seism. Soc. Am.* **87,** 396–413.

Rotstein, Y., and A. L. Kafka (1982). Seismotectonics of the southern boundary of Anatolia, eastern Mediterrenean region: subduction, collision, and are jumping, *J. Geophys. Res.* **87,** 7694–7706.

Ruzaikin, A. I., I. L. Nersesov, V. I. Khalturin, and P. Molnar (1977). Propagation of Lg and lateral variations of crustal structure in Asia, *J. Geophys. Res.* **82,** 307–316.

Sandvol, E., K. Al-Damegh, A. Calvert, D. Seber, M. Barazangi, R. Mohamad, R. Gok, N. Turkelli, and C. Gurbuz (2001). Tomographic

imaging of observed regional wave propagation in the Middle East, *Pure Appl. Geophys.* **158,** 1121–1163.

Seber, D., M. Barazangi, A. Ibenbrahim, and A. Demnati (1996). Geophysical evidence for lithospheric delamination beneath the Alboran Sea and Rif-Betic mountains, *Nature* **379,** 785–790.

Şengör, A. M. C., and W. S. F. Kidd (1979). Post-collisional tectonics of the Turkish-Iranian Plateau and a comprasion with Tibet, *Tectonophysics* **55,** 361–376.

Şengör, A. M. C., S. Özeren, T. Genç, and E. Zor (2003). East Anatolian high plateau as a mantle-supported, N-S shortened domal structure, *Geophys. Res. Lett.* **30,** 8044, doi 10.1029/2003GL017858.

Taylor, S. R., X. Yang, and W. S. Philips (2003). Bayesian Lg attenuation tomography applied to Eastern Asia, *Bull. Seism. Soc. Am.* **93,** 795–803.

Whitney, D. L., and M. A. Hamilton (2004). Timing of high grade metamorphism in central Turkey and the assembly of Anatolia, *J. Geol. Soc.* **161,** 823–828.

Xie, J., and B. J. Mitchell (1990a). A back projection method for imaging large scale lateral variation in Lg coda Q with application to continental Africa, *Geophys. J. Int.* **100,** 161–181.

Xie, J., and B. J. Mitchell (1990b). Attenuation of multiphase surface waves in the Basin and Range province I, Lg and Lg coda, *Geophys. J. Int.* **102,** 121–137.

Xie, J., and O. W. Nuttli (1988). Interpretation of high-frequency coda at large distances: stochastic modelling and method of inversion, *Geophys. J. Int.* **95,** 579–585.

Xie, J., R. Gok, J. Ni, and Y. Aoki (2004). Lateral variations of crustal seismic attenuation along the INDEPTH profiles in Tibet from Lg Q inversion, *J. Geophys. Res.* **109,** B10308, doi 10.1029/2004JB002988.

Zhu, L., B. Mitchell, N. Akyol, I. Cemen, and K. Kekovali (2006). Crustal thickness variation in the Aegean region and its implications for the extension of continental crust, *J. Geophys. Res.* **111,** doi 10.1029/2005JB003770.

Zor, E., E. Sandvol, C. Gurbuz, N. Turkelli, D. Seber, and M. Barazangi (2003). The crustal structure of the East Anatolian plateau from receiver functions, *Geophys. Res. Lett.* **30,** 8044, doi 10.1029/2003GL018192.

Department of Geological Sciences
University of Missouri
Columbia, Missouri 65211
(E.Z., E.S.)

Lamont-Doherty Earth Observatory
Columbia University
Palisades, New York 10964-8000
(J.X.)

Kandilli Observatory and Earthquake Research Ins.
Boğaziçi University
Çengelköy, Istanbul, Turkey 81220
(N.T.)

Earth and Atmospheric Sciences
Saint Louis University
St. Louis, Missouri 63103
(B.M.)

Republican Center of Seismic Survey
Azerbaijanian Academy of Sciences
Nydar Rabybaylee St., 370001, Baku, Azerbaijan
(A.G., G.Y.)

Manuscript received 11 November 2005.